Department of Information Technology and Mathematical Methods

Working Paper

Series "*Mathematics and Statistics*"

On the physical consistency of the coupling

between three-dimensional compliant

and one-dimensional problems in haemodynamics

by

L. Formaggia, A. Quarteroni, C. Vergara

COMITATO DI REDAZIONE[§]

Series Information Technology (IT): Stefano Paraboschi
Series Mathematics and Statistics (MS): Luca Brandolini, Ilia Negri

On the physical consistency of the coupling between three-dimensional compliant and one-dimensional problems in haemodynamics [*]

Luca Formaggia[†], Alfio Quarteroni[‡], Christian Vergara[§]

Abstract

In this work we discuss the reliability of the coupling among three-dimensional (3D) and one-dimensional (1D) models, that describe blood flowing into the circulatory tree. In particular, we study the physical consistency of the 1D model with respect to the 3D one. To this aim, we introduce a general criterion based on energy balance for the proper choice of coupling conditions between models. We also propose a way to include in the 1D model the effect of the external tissue surrounding the vessel and we discuss its importance whenever this effect is considered in the 3D model. Finally, we propose several numerical results in real human carotids, studying different configurations for the 1D model and highlighting the best one in view of the physical consistency.

Keywords: Cardiovascular simulation, geometrical multiscale, total pressure, surrounding tissue, human carotid.

1 Introduction

The cardiovascular system is formed by a complex network of vessels where local and global phenomena influence each other. Modeling with different degree of detail is therefore mandatory to obtain physiological and patient-specific results. In this context, it has been proposed in the last decade to couple heterogeneous models characterized by different spatial dimension, leading to a *geometrical multiscale* approach. The main idea underlying this strategy is to focus on a specific district of interest, where we want to have a three-dimensional (3D) accurate description, and to *embed* it in a net of one-dimensional (1D) and/or zero-dimensional (0D) models, which take into account for the rest of the circulatory tree and provide suitable boundary conditions to the 3D model. This idea has been first proposed in [26] and it has been then developed and studied also in other works and by other groups, we mention for example [13, 25, 22, 27, 29, 2, 21].

[†]MOX, Dipartimento di Matematica, Politecnico di Milano, Italy, `luca.formaggia@polimi.it`

[‡]SB MATHICSE CMCS, EPF de Lausanne, Switzerland; MOX, Dipartimento di Matematica, Politecnico di Milano, Italy, `alfio.quarteroni@epfl.ch`

[§]Dipartimento di Ingegneria dell'Informazione e Metodi Matematici, Università degli Studi Bergamo, Italy, `christian.vergara@unibg.it`

Among the different strategies, a particular attention has been paid to the 3D-1D coupling, based on the interaction between a 3D model of blood in a compliant vessel and a net of 1D models to account for a larger part of the vascular tree [9, 12, 3, 17]. For the 3D model it is necessary to consider a fluid-structure interaction (FSI) problem, since blood flow is coupled with the deformation of the arterial wall.

The 1D network is composed by connecting 1D models, each of them describing the flow in a single vessel. They are derived by integration of the Navier-Stokes equations written in a moving domain over sections orthogonal to the axial direction. The hypotheses underlying the derivation of the 1D model, that trace back to the seminal work of Leonhard Euler in 1775 [8], are: i) the fluid domain at rest is a cylinder; ii) the structure is assumed to be a linear *membrane*, with a normal wall displacement. The 1D model can therefore be regarded as a spatially reduced 3D-FSI model, consisting of a straight cylinder surrounded by a linear membrane structure. Therefore, the 1D model cannot provide insightful information about the local fluid-dynamics, but it generates an average solution along the axial vessel's coordinate. In particular it is able to describe flow rate distributions and pressure wave propagation. It is therefore reasonable to ask whether the 1D model can reproduce physiological results with reasonable accuracy, when used as an approximation of a 3D real vessel geometry with a thick wall. We refer to this topic as *physical consistency* of the 1D model with respect to a 3D-FSI one. Of course, the fulfillment (in a suitable sense) of the physical consistency is a major issue to obtain reliable results when one considers a 3D-1D coupled system.

In this work, we provide three different analyses in the direction of assessing the physical consistency of the 1D model. The first aims to investigate which coupling conditions at the interface between 3D-FSI and 1D models guarantee the satisfaction of physical principles based on energy balance (topic I). In fact, it is known that the 3D-FSI model and the 1D model separately satisfy an energy inequality. Here, we investigate when a global energy estimate holds too.

The second aim of the work is to consider the tissue surrounding the vessel in the 1D model (topic II). In the 3D-FSI model, the presence of the external tissue is often modeled by providing the outer surface of the arterial wall with suitable boundary conditions that "mimic" the action of the surrounding tissue. Recently, a Robin boundary condition has been proposed under the assumption that the external environment exerts an elastic feedback on the artery wall [23, 6, 24]. Here, we include this modelization in the 1D model, through the derivation of an equivalent elastic constant, that accounts for the external tissue.

The third aim of the work consists in performing numerical simulations in real geometries, using a set of coupling conditions satisfying the above energy principle. This set of numerical experiments aims at quantifying the discrepancy between the results obtained with the full 3D model and those obtained by using the coupled 3D-1D one (topic III). Little has been done so far in this direction. In [12] a comparison between a full 3D model of a cylinder with a thick linear structure, and a system obtained by coupling half of the 3D model with a 1D model was considered. The authors showed that in this case the coupled system leads to accurate results with respect to those obtained with the full 3D system. In [3], a comparison has been performed between a 3D model of a femoral artery

2

with a membrane structure and the system obtained by coupling half of the latter with a 1D model. The authors found that the coupled model is quite accurate, being the relative error with respect to the full 3D model of the quantities of interest less than 5%. The results in [12, 3] highlight the effectiveness of the 3D-FSI/1D coupling in two different cases: that of a cylindrical domain with a thick structure, or the one of a real complex geometry with a membrane structure. Here we want to make the additional step of analyzing the accuracy of the 3D-FSI/1D coupled model for a real 3D geometry with thick structure. To this aim, we report several numerical results obtained in human carotids.

The main results achieved by this work are briefly described in what follows. Regarding topic I, we found that the classical coupling conditions based on the continuity of the flow rate and of the mean pressure are not in general energy preserving, differently than those based on the continuity of the flow rate and of the *mean total pressure*. As for topic II, we found that the effect of the surrounding tissue could be accounted for in the 1D case by suitably modifying the Young modulus, by adding a term proportional to the elasticity of the surrounding tissue. The numerical experiments showed that the inclusion of this correction is crucial in order to yield meaningful results. Finally, regarding topic III, we found that by considering tapering in the 1D model representing the branch cut from the 3D model, the accuracy with respect to the full 3D model considerably improves.

The outline of the paper is as follows. In Section 2, we introduce separately the 3D-FSI and the 1D models, whilst in Section 3 we discuss which sets of coupling conditions satisfy a physical principle based on energy dissipation. In Section 4, we discuss the effect of accounting for the surrounding tissue in the 1D model, and we show some related numerical results in Section 5.1 in order to study the effect of neglecting this correction. Finally in Section 5.2 we show several numerical results in real geometries with the aim at investigating the physical consistency of the 3D-FSI/1D coupled system.

2 Problem setting

2.1 The 3D fluid-structure interaction problem

We consider problems defined on tubular domains, like the one depicted in Figure 1, representing a portion of the arterial tree, and formed by a fluid part Ω_f^t, the lumen, and a structural part Ω_s^t, the vessel wall, both open subsets of $\mathbb{R}^3$. The superscript t indicates that they are changing with time, as they correspond to the current configuration at time t. We indicate with Σ^t the interface between the two domains, $\Sigma^t = \partial\Omega_f^t \cap \partial\Omega_s^t$. The sections that artificially separate the arterial section at hand from the remaining part of the arterial tree are indicated with $\Sigma_{f,i}^t$ and $\Sigma_{s,i}^t$, for the fluid and structure, respectively. The external boundary is Σ_{out}^t, and involves only the structural part.

Blood velocity is denoted by $\boldsymbol{u}_f = \boldsymbol{u}_f(\boldsymbol{x}, t)$, the fluid pressure by $p = p(\boldsymbol{x}, t)$, while $\boldsymbol{\eta}_s = \boldsymbol{\eta}_s(\boldsymbol{x}, t)$ is the structure displacement. Since we work in a moving domain, the fluid problem is stated in an *Arbitrary Lagrangian-Eulerian* (ALE) framework (see e.g. [19, 7]), while we adopt the common Lagrangian approach for the structure. At every time t, the ALE map $\mathcal{A}^t$ is an appropriate lifting into the fluid domain of the structure displacement
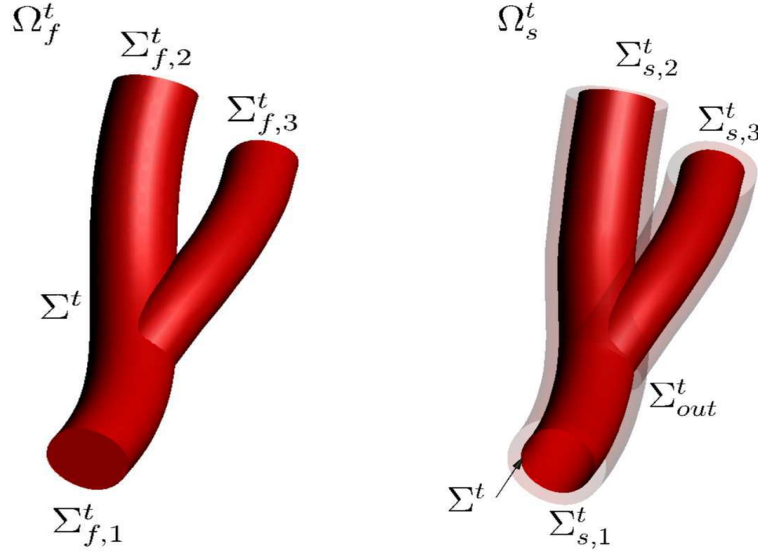
3

Figure 1: Representation of the domain of the FSI problem: fluid domain on the left, structure domain on the right.

at the fluid-structure interface Σ^t. It defines the displacement $\boldsymbol{\eta}_m$ of points in Ω_f^t during the movement of the fluid domain with respect to a reference configuration $\widetilde{\Omega}_f$. Its time derivative is the fluid domain velocity $\boldsymbol{u}_m$. The ALE time derivative of a function f in Ω_f^t is then defined as

$$\frac{D^A f}{Dt} = \frac{\partial f}{\partial t} + (\boldsymbol{u}_m \cdot \nabla)f.$$

The ALE frame is functional to the numerical discretization because it allows to conveniently express the time variation of relevant quantities at the nodes of the computational mesh, which is moving with the domain.

The incompressible Navier-Stokes equations for a homogeneous and Newtonian fluid are assumed to hold in Ω_f^t, and we indicate with $\boldsymbol{T}_f$ the related Cauchy stress tensor defined by

$$\boldsymbol{T}_f(\boldsymbol{u}, p) := -p\boldsymbol{I} + 2\mu\boldsymbol{D}(\boldsymbol{u}),$$

where

$$\boldsymbol{D}(\boldsymbol{u}) = \frac{1}{2}\left(\nabla\boldsymbol{u} + (\nabla\boldsymbol{u})^T\right)$$

is the strain rate tensor.

To describe the structure kinematics we adopt a genuine Lagrangian approach. With $\widetilde{\Omega}_s$ we denote the reference configuration for the solid part, assumed to be a natural state, and the displacement $\boldsymbol{\eta}_s$ is taken with respect to this configuration. Whenever not clear

4

by the context we use the symbol $\sim$ to indicated quantities pushed back to the reference configuration. In particular, we indicate with $\widetilde{\boldsymbol{P}}_s$ the first Piola-Kirchoff stress tensor, linked to the Cauchy stress tensor $\boldsymbol{T}_s = \boldsymbol{T}_s(\widetilde{\boldsymbol{\eta}}_s)$ by

$$\widetilde{\boldsymbol{P}}_s = J\boldsymbol{T}_s\boldsymbol{F}^{-T},$$

where $J = \det(\boldsymbol{F})$ and $\boldsymbol{F} = \boldsymbol{I} + \nabla\widetilde{\boldsymbol{\eta}}_s$ are the Jacobian of the Lagrangian map and the deformation gradient, respectively. For a hyper-elastic material the first Piola-Kirchoff tensor is expressed as function of the Green-Lagrange stress tensor

$$\boldsymbol{E} = \frac{1}{2}(\boldsymbol{F}^T\boldsymbol{F} - \boldsymbol{I}) = \frac{1}{2}(\nabla\widetilde{\boldsymbol{\eta}}_s + \nabla^T\widetilde{\boldsymbol{\eta}}_s) + \frac{1}{2}\nabla^T\widetilde{\boldsymbol{\eta}}_s\widetilde{\boldsymbol{\eta}}_s$$

as

$$\widetilde{\boldsymbol{P}}_s = \boldsymbol{F}\frac{\partial W}{\partial \boldsymbol{E}},$$

W being a suitable density of elastic energy. For arteries, several elastic energy functions have been proposed so far, in particular *neo-Hookian* and *exponential* materials have been mainly considered, see for example [16, 18, 28]. For a homogeneous elastic material we have

$$\widetilde{\boldsymbol{T}}_s(\widetilde{\boldsymbol{\eta}}_s) = \frac{E}{2(1+\nu)}\boldsymbol{E}(\widetilde{\boldsymbol{\eta}}_s) + \frac{E\nu}{(1+\nu)(1-2\nu)}\operatorname{tr}(\boldsymbol{E}(\widetilde{\boldsymbol{\eta}}_s))\,\boldsymbol{I}, \tag{1}$$

where E is the Young modulus and ν the Poisson ratio.

The fluid-structure interaction (FSI) problem is therefore governed by the following differential problems:

1. *Fluid-Structure interaction.* Given the (unknown) fluid domain velocity $\boldsymbol{u}_m$ and fluid domain Ω_f^t, find, at each time $t \in (0, T]$, fluid velocity $\boldsymbol{u}_f$, pressure p and structure displacement $\boldsymbol{\eta}_s$ such that

$$\begin{cases} \rho_f\dfrac{D^A\boldsymbol{u}_f}{Dt} + \rho_f((\boldsymbol{u}_f - \boldsymbol{u}_m)\cdot\nabla)\boldsymbol{u}_f - \nabla\cdot\boldsymbol{T}_f(\boldsymbol{u}_f, p) = \boldsymbol{0} & \text{in } \Omega_f^t, \\ \nabla\cdot\boldsymbol{u}_f = 0 & \text{in } \Omega_f^t, \\ \widetilde{\rho}_s\dfrac{\partial^2\widetilde{\boldsymbol{\eta}}_s}{\partial t^2} - \nabla\cdot\widetilde{\boldsymbol{P}}_s(\widetilde{\boldsymbol{\eta}}_s) = \boldsymbol{0} & \text{in } \widetilde{\Omega}_s, \end{cases} \tag{2}$$

where ρ_f and $\widetilde{\rho}_s$ are the fluid and structure density, respectively, the latter referred to the reference configuration. We also consider the following interface conditions

$$\begin{cases} \boldsymbol{u}_f = \dfrac{\partial\boldsymbol{\eta}_s}{\partial t} & \text{on } \Sigma^t, \\ \boldsymbol{T}_s(\boldsymbol{\eta}_s)\,\boldsymbol{n}_s + \boldsymbol{T}_f(\boldsymbol{u}_f, p)\,\boldsymbol{n}_f = \boldsymbol{0} & \text{on } \Sigma^t, \end{cases} \tag{3}$$

stating the continuity of velocity and normal stresses at the FS interface. We indicate with $\boldsymbol{n}$ the outward normal to the domain boundary, yet when there is ambiguity, as in the previous expression, we add the suffix s or f to mark the fluid or the structural domain, respectively. Furthermore we will consider the following boundary Robin-type condition on $\widetilde{\Sigma}_{out}$,

$$\alpha_e\widetilde{\boldsymbol{\eta}}_s + \widetilde{\boldsymbol{P}}_s(\widetilde{\boldsymbol{\eta}}_s)\,\widetilde{\boldsymbol{n}} = P_{ext}\widetilde{\boldsymbol{n}}, \qquad \text{on } \widetilde{\Sigma}_{out}, \tag{4}$$

5

where P_{ext} is a given external pressure distribution, while α_e is a non-negative constant. This condition simulates the presence of an elastic external tissue, α_e being the elastic coefficient (see [23, 20]).

2. *Geometry problem.* Given the (unknown) interface structure displacement $\widetilde{\boldsymbol{\eta}}_s|_{\widetilde{\Sigma}}$, find by a suitable extension of this datum, the displacement of the fluid domain $\boldsymbol{\eta}_m$, for instance by solving

$$\begin{cases} -\triangle\widetilde{\boldsymbol{\eta}}_m = \widetilde{\boldsymbol{0}} & \text{in } \widetilde{\Omega}_f, \\ \widetilde{\boldsymbol{\eta}}_m = \widetilde{\boldsymbol{\eta}}_s & \text{on } \widetilde{\Sigma}, \end{cases} \tag{5}$$

and then find accordingly the fluid domain velocity $\widetilde{\boldsymbol{u}}_m = \frac{\partial\widetilde{\boldsymbol{\eta}}_m}{\partial t}$. A point $\boldsymbol{x}_f \in \Omega_f^t$ is related to the corresponding point $\widetilde{\boldsymbol{x}}_f$ of the reference domain $\widetilde{\Omega}_f$ by

$$\boldsymbol{x}_f = \widetilde{\boldsymbol{x}}_f + \widetilde{\boldsymbol{\eta}}_m.$$

Equations (2) and (5) have to be endowed with suitable boundary conditions at $\Sigma_{f,i}$ and $\Sigma_{s,i}$ and initial conditions for $\boldsymbol{u}_f$, $\widetilde{\boldsymbol{\eta}}_s$ and $\dfrac{\partial\widetilde{\boldsymbol{\eta}}_s}{\partial t}$. They are not discussed here, rather, they will be described case by case in the numerical results.

2.2 The one-dimensional reduced model

Referring to the compliant cylinder in Figure 2, whose length is L, a simplified 1D model can be obtained integrating at each time t the Navier-Stokes equations over each section S normal to the axis z of the cylinder. The 1D model reads, for each $t > 0$ and $0 < z < L$, (see [9, 13])

$$\begin{cases} \dfrac{\partial A}{\partial t} + \dfrac{\partial Q}{\partial z} = 0, \\ \dfrac{\partial Q}{\partial t} + \dfrac{\partial}{\partial z}\Big(\alpha\dfrac{Q^2}{A}\Big) + \dfrac{A}{\rho_f}\dfrac{\partial P}{\partial z} + K_r\dfrac{Q}{A} = 0, \end{cases} \tag{6}$$

where Q is the flow rate through S, A is the area of S, P the mean pressure over S, K_r is a resistance parameter which accounts for the fluid viscosity, while α accounts for the shape of the velocity profile over S. From now on, variables which in principle take different values in the 3D-FSI and in the 1D models are denoted with symbol $\widehat{\ }$ when belonging to the 1D model. System (6) is a system of two equations in three unknowns
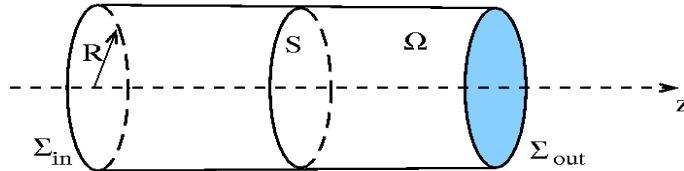

Figure 2: Reference cylinder Ω.

(P, Q, A). For its closure, a third equation is provided by a suitable wall model relating

6

the radial displacement (and therefore the area A) to the mean pressure P. In particular, we consider the general law

$$P = P_{ext} + \psi(A), \quad \frac{d\psi}{dA} > 0, \quad \psi(\widetilde{A}) = 0, \tag{7}$$

where $\widetilde{A}$ is the area of the surface S at $t = 0$. A classical choice is to consider an algebraic law of the type

$$\psi(A) = \beta(A)\frac{\sqrt{A} - \sqrt{\widetilde{A}}}{\sqrt{\pi}}, \tag{8}$$

where

$$\beta = \frac{\widehat{H}_s \widehat{E}\,\pi}{(1 - \widehat{\nu}^2)A}, \tag{9}$$

being $\widehat{H}_s$ the thickness of the structure, and $\widehat{E}$ and $\widehat{\nu}$ the Young modulus and Poisson ratio, respectively. $\widehat{H}_s$ and $\widehat{E}$ (and therefore β) could in principle be functions of z, whilst it is a common practice to use constant values over time. In particular, in this work we use $\beta = \beta(\widetilde{A})$ for the numerical experiments.

The characteristic variables related to the 1D reduced model (6), (7), (8) are given by (see [9])

$$W_{1,2} = \frac{Q}{A} \pm 4\gamma\left(A^{1/4} - A_0^{1/4}\right),$$

where $\gamma = \sqrt{\frac{\beta}{2\rho_f \pi}}$. With the choices (7)-(8), it is possible to show that system (6) is hyperbolic and possesses two distinct eigenvalues [15]

$$\lambda_{1,2} = \frac{Q}{A} \pm \gamma\,A^{1/4}.$$

Under physiological conditions the flow is sub-critical, so that the eigenvalues have opposite sign, $\lambda_1 > 0$ and $\lambda_2 < 0$. In this case, W_1 corresponds to the incoming characteristic on the point $z = 0$, while W_2 is the incoming characteristic in the point $z = L$.

3 Energy invariant coupling conditions

Once we have at disposal a 3D-FSI and a 1D system, we would like to use them in a coupled way as a simplified model of a full 3D-FSI one. The coupled model is obtained by substituting a part of 3D-FSI with a 1D model. In order to guarantee that the coupled model features accurate results, we have to show that a "physical consistency" property holds. In other words, it is necessary to understand when the coupled model reproduces solutions which are in agreement (in some suitable sense) with those obtained by the full system. To this aim, we here analyze possible couplings between the 3D-FSI and the 1D models from the point of view of energy estimates. We start considering a simplified setting, the found result can however be extended to more general situations. Let us consider a single 3D elastic pipe $\mathcal{P}$ modeling an artery and the differential problem provided
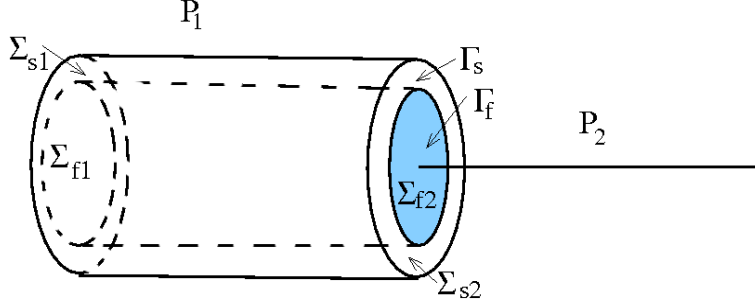
Figure 3: Schematic representation of the coupling between the 3D ($\mathcal{P}_1$) and the 1D ($\mathcal{P}_2$) models.

by (2), (3), (4) and (5). For the scope of this section we consider homogeneous Dirichlet boundary conditions for both fluid velocity and structure displacement at the artificial sections, and a non null initial condition. It is well known that a solution of the FSI problem under the stated conditions satisfies an energy decay property [14, Chapter 9]. We now split the pipe along its axis into two parts, $\mathcal{P}_1$ and $\mathcal{P}_2$, then we replace $\mathcal{P}_2$ with the corresponding 1D model. For simplicity, we set the origin of the axis so that $z \in (0, L)$ in the 1D model, L being the length of $\mathcal{P}_2$. We will use then the same notation adopted in the previous section to denote the various portions of the boundary of $\mathcal{P}_1$. The interface between models is given by $\Gamma^t = \Gamma^t_f \cup \Gamma^t_s$ for the 3D model, and $z = 0$ for the 1D one. In the example depicted in Figure 3, we have $\Gamma^t_f = \Sigma^t_{f,2}$ and $\Gamma^t_s = \Sigma^t_{s,2}$.

The 3D-FSI model lies in $\mathcal{P}_1$, and is governed by equations (2), (3), (4) and (5), with Dirichlet boundary conditions

$$
\begin{aligned}
\boldsymbol{u}_f &= \boldsymbol{0} && \text{on } \partial\Omega^t_f \setminus (\Sigma^t \cup \Gamma^t_f) && t > 0, \\
\boldsymbol{\eta}_s &= \boldsymbol{0} && \text{on } \partial\Omega^t_s \setminus (\Sigma^t \cup \Gamma^t_s) && t > 0,
\end{aligned}
\tag{10}
$$

while for the 1D model we set

$$
Q = 0 \quad \text{at } z = L. \tag{11}
$$

We leave unspecified for now the conditions at the interface Γ^t between models.

The proposed model problem still should simulate the flow in pipe $\mathcal{P}$. Thus we wish that a solution of the coupled problem satisfies an energy inequality akin to that of the complete model and find interface conditions that do not affect the energy balance of the system.

To this aim we define the following total energy of the 3D fluid-structure problem

$$
\mathcal{E}^{3D}(t) = \frac{\rho_f}{2} \int_{\Omega^t_f} |\boldsymbol{u}_f(t, \boldsymbol{x})|^2 \, d\Omega + \int_{\widetilde{\Omega}_s} \frac{\rho_s}{2} |\dot{\widetilde{\boldsymbol{\eta}}}_s(t, \boldsymbol{x})|^2 \, d\Omega + \int_{\widetilde{\Omega}_s} W(\boldsymbol{E}(t, \boldsymbol{x})) \, d\Omega + \int_{\widetilde{\Gamma}_{out}} \alpha_e |\widetilde{\boldsymbol{\eta}}_s(t, \boldsymbol{x})|^2 d\gamma,
$$

and the following total energy of the 1D model [9]

$$
\mathcal{E}^{1D}(t) = \frac{\rho_f}{2} \int_0^L A(t, x) \, U^2(t, x) \, dx + \int_0^L \Psi(A(t, x)) \, dx,
$$

8

where $U := \frac{Q}{A}$ is the mean velocity, and $\Psi(A) = \int_{A_0}^{A} \psi(\tau)\, d\tau$. For the sake of notation, in what follows we highlight the dependence of variables just with respect to time.

Proposition 1. *A solution of the 3D-FSI problem under conditions (10) satisfies the following energy equality*

$$\frac{d}{dt}\mathcal{E}^{3D}(t) + 2\mu \int_{\Omega_f^t} |\boldsymbol{D}(\boldsymbol{u}_f(t))|^2 \, d\Omega + \int_{\widetilde{\Gamma}_{out}} \alpha_e |\dot{\widetilde{\boldsymbol{\eta}}}_s(t)|^2 d\gamma = \int_{\Gamma^t} \boldsymbol{T}_f(\boldsymbol{u}_f(t), p_{tot}(t))\boldsymbol{n} \cdot \boldsymbol{u}_f(t)\, d\gamma$$

$$+ \int_{\Gamma^t} \boldsymbol{T}_s(\boldsymbol{\eta}_s(t))\boldsymbol{n} \cdot \dot{\boldsymbol{\eta}}_s(t)\, d\gamma. \quad (12)$$

Here $p_{tot} := p + \frac{\rho_f}{2}|\boldsymbol{u}_f|^2$ is the fluid total pressure.

The proof is rather standard and is based on multiplying the momentum equation for the fluid by $\boldsymbol{u}_f$, the equation for the structure by $\dot{\widetilde{\boldsymbol{\eta}}}_s$, followed by a formal manipulation of the integrals using Gauss theorem and the enforcement of the given boundary conditions.

Proposition 2. *The 1D problem under conditions (11) satisfies the following energy equality*

$$\frac{d}{dt}\mathcal{E}^{1D}(t) + \rho_f K_r \int_0^L U(t)^2 \, dx = Q(t)|_{z=0}\, P_{tot}(t)|_{z=0}, \quad (13)$$

where $P_{tot} = P + \frac{\rho_f}{2}U^2$, is the total pressure in the 1D model.

The demonstration may be found in [9]. We have then the following

Proposition 3. *If the interface conditions are such that*

$$\Delta\mathcal{E}(t) = \int_{\Gamma_f^t} \boldsymbol{T}_f(\boldsymbol{u}_f(t), p_{tot}(t))\boldsymbol{n} \cdot \boldsymbol{u}_f(t)\, d\gamma + \int_{\Gamma_s^t} \boldsymbol{T}_s(\boldsymbol{\eta}_s(t))\boldsymbol{n} \cdot \dot{\boldsymbol{\eta}}_s(t)\, d\gamma + Q(t)|_{z=0}P_{tot}(t)|_{z=0} \leq 0$$

$$(14)$$

for all $t > 0$, then the coupled 3D-FSI/1D problem satisfies the energy decay property

$$\frac{d}{dt}\left(\mathcal{E}^{3D}(t) + \mathcal{E}^{1D}(t)\right) \leq 0$$

for all $t > 0$.

Proof. It is sufficient to sum (12) and (13) member by member and apply condition (14). □

If the interface conditions are such that $\Delta\mathcal{E} \leq 0$ for all allowable values of pressure, velocity and displacements, then we say that they are *energy dissipating*. Moreover, interface conditions that satisfy the stronger requirement $\Delta\mathcal{E} = 0$ (which is physically justified), will be called *energy preserving* interface conditions.

Proposition 4. *The following interface conditions*

$$\begin{cases} \int_{\Gamma_f^t} \boldsymbol{u}_f(t) \cdot \boldsymbol{n} \, d\gamma = Q(t)|_{z=0}, \\ \left(\boldsymbol{T}_f(\boldsymbol{u}_f(t), p_{tot}(t)) \boldsymbol{n} \right) |_{\Gamma_f^t} = -P_{tot}(t)|_{z=0} \boldsymbol{n}, \end{cases} \tag{15}$$

for the fluid part, joined with either

$$\boldsymbol{T}_s(\boldsymbol{\eta}_s) \boldsymbol{n} = \boldsymbol{0} \quad at \ \Gamma_s^t, \tag{16}$$

or

$$\begin{cases} \boldsymbol{\eta}_s \cdot \boldsymbol{n} = \boldsymbol{0} & at \ \Gamma_s^t, \\ (\boldsymbol{T}_s(\boldsymbol{\eta}_s) \boldsymbol{n}) \times \boldsymbol{n} = \boldsymbol{0} & at \ \Gamma_s^t, \end{cases} \tag{17}$$

for the structure, are energy preserving.

Proof. To prove this statement we first analyze conditions (15). By using both $(15)_1$ and $(15)_2$ and by noticing that $\boldsymbol{T}_f(\boldsymbol{u}_f, p_{tot}) \boldsymbol{n}$ is aligned with the normal direction and constant over Γ_f^t, we obtain

$$\int_{\Gamma_f^t} \boldsymbol{T}_f(\boldsymbol{u}_f(t), p_{tot}(t)) \boldsymbol{n} \cdot \boldsymbol{u}_f(t) \, d\gamma = -P_{tot}(t)|_{z=0} \int_{\Gamma_f^t} \boldsymbol{u}_f(t) \cdot \boldsymbol{n} \, d\gamma = -P_{tot}(t)|_{z=0} Q(t)|_{z=0},$$

so that from (14) we have

$$\Delta \mathcal{E}(t) = \int_{\Gamma_s^t} \boldsymbol{T}_s(\boldsymbol{\eta}_s(t)) \boldsymbol{n} \cdot \dot{\boldsymbol{\eta}}_s(t) \, d\gamma.$$

This term is clearly null if (16) is true. To show that it is still zero if when considering (17) instead of (16), it is sufficient to note that conditions (17) imply $\dot{\boldsymbol{\eta}}_s \cdot \boldsymbol{n} = 0$, and thus $\dot{\boldsymbol{\eta}}_s = \boldsymbol{n} \times \dot{\boldsymbol{\eta}}_s \times \boldsymbol{n}$. Consequently, we obtain

$$\int_{\Gamma_s^t} \boldsymbol{T}_s(\boldsymbol{\eta}_s(t)) \boldsymbol{n} \cdot \dot{\boldsymbol{\eta}}_s(t) \, d\gamma = \int_{\Gamma_s^t} \dot{\boldsymbol{\eta}}_s(t) \cdot [\boldsymbol{T}_s(\boldsymbol{\eta}_s(t)) \boldsymbol{n} \times \boldsymbol{n}] \times \boldsymbol{n} \, d\gamma = 0,$$

where we have used the algebraic identity $\boldsymbol{a} \cdot (\boldsymbol{b} \times \boldsymbol{c}) = \boldsymbol{c} \cdot (\boldsymbol{a} \times \boldsymbol{b})$. $\square$

The first condition in (15) states the continuity of mass flux, the second that of total normal stresses, which are taken constant on the 3D part of the interface Γ_f^t. The two alternative conditions (16) and (17) on the structural part of the interface specify zero normal stresses (homogeneous Neumann) or null tangential component of the normal stresses and no normal displacement, respectively. We may note that there is no direct coupling between the 3D structure and the 1D model. This fact reflects that the simplified structural law used in the 1D model is unable to provide enough information to feed the structural part of the 3D-FSI model. In particular, the above conditions do not imply continuity of the section area, i.e. in general $A \neq \int_{\Gamma_f} d\gamma$. We wish to point out that the lack of continuity of the section area at the interface does not imply that the 3D and 1D structural models are uncoupled. The evolution of the section area in the 3D model depends on the stress field acting on the structure, which is linked to the pressure in the 1D model (and then to the 1D structure) thanks to the second of (15).

Remark 1. *The interface conditions analyzed in Proposition 4 are not the only set of energy preserving conditions. Indeed, one may replace the last of (17) with $\boldsymbol{\eta}_s = \mathbf{0}$ on Γ_s^t. The latter, however, is physically less justifiable, since it implies that Γ_s remains fixed.*

Remark 2. *Interface conditions based on the total pressure have been already considered in [11] for the 1D/1D coupling and in [12] for the 3D-FSI/1D coupling. In the latter work the authors used, for stability purposes, a particular treatment of the convective term in the Navier-Stokes equations, which leads naturally to conditions on the total pressure. Here, we advocate the use of total pressure as energy preserving conditions independently of the formulation adopted for the Navier-Stokes problem.*

Remark 3. *For practical reasons of implementation, it may be desirable to replace (15) with*

$$\begin{cases} \displaystyle\int_{\Gamma_f^t} \boldsymbol{u}_f(t) \cdot \boldsymbol{n}\, d\gamma = Q(t)|_{z=0}, \\ \left(\boldsymbol{T}_f(\boldsymbol{u}_f(t), p(t))\boldsymbol{n}\right)|_{\Gamma_f^t} = -P(t)|_{z=0}\boldsymbol{n}, \end{cases} \tag{18}$$

which involves in the second equation the pressure instead of total pressure. Exploiting the definition of P_{tot} and considering for the structure either (16) or (17), we have from (14) that

$$\Delta\mathcal{E}(t) = \frac{\rho_f}{2}\left(Q(t)|_{z=0}\left(U(t)|_{z=0}\right)^2 - \int_{\Gamma_f^t} |\boldsymbol{u}_f(t)|^2 \boldsymbol{u}_f(t) \cdot \boldsymbol{n}\, d\gamma \right),$$

whose sign is not defined in general. It follows that interface conditions (18) may jeopardize the fulfillment of an energy inequality and consequently lead to a possible loss of stability of the coupled problem.

The considerations here made for a single interface can be readily extended to the case of several interfaces, leading to analogous conditions.

4   Modeling the surrounding tissue in the 1D model

In order to find a physically consistent 1D model, it is natural to use the same Poisson ratio for the 3D-FSI and the 1D models, that is $\widehat{\nu} = \nu$. Ragarding the Young modulus, we should also account for the presence of the surrounding tissue. In the 3D-FSI the absence of the external environment was surrogated by Robin condition (4). This is not the case in the standard derivation of the 1D model. Therefore, the choice $\widehat{E} = E$ does not seem to be the proper one. In what follows, we examine how the presence of the external tissue may be modeled in the 1D model, and consequently how $\widehat{E}$ could be chosen. To start with, we note that in the derivation of the 1D model the structure is regarded as a membrane and therefore geometrically is a surface, coinciding with its external surface. We also point out that both the surrounding tissue and the 1D vessel law are described through a linear algebraic law between the pressure and the displacement, through (4) and (8), respectively. Therefore, we can derive an equivalent model by considering the situation depicted in Figure 4, where the stifness of the arterial wall and that of the surrounding tissue is
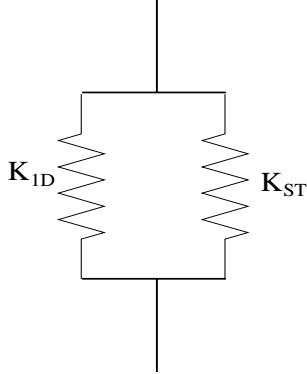
Figure 4: Representative equivalent scheme of the 1D model in presence of surrounding tissue (ST). K_{1D} represents the elastic constant of the 1D model without considering ST, whilst K_{ST} represents that of ST.

modeled by two springs in parallel. In particular, by denoting K_{1D} the elastic constant of the 1D vessel model without surrounding tissue and K_{ST} that of the surrounding tissue, we have that the equivalent elastic constant is given by $K_{eq} = K_{1D} + K_{ST}$. From (8), it follows that $K_{1D} = \beta(E)$, where we have highlighted the dependence of β on the Young modulus E, see (9). Furthermore, from (4) it follows that $K_{ST} = \alpha_e$. Therefore, the equivalent Young modulus $\widehat{E}$, by which the 1D model is equivalent to the 3D-FSI model with surrounding tissue, has to satisfy

$$K_{eq} = \beta(\widehat{E}) = \frac{\widehat{H}_s \widehat{E} \pi}{(1 - \nu^2)\widetilde{A}} = \frac{\widehat{H}_s E \pi}{(1 - \nu^2)\widetilde{A}} + \alpha_e.$$

This yields

$$\widehat{E} = E + \frac{(1 - \nu^2)\widetilde{A}}{\widehat{H}_s \pi}\alpha_e, \tag{19}$$

which corresponds to an increase of the stiffness in the 1D model.

5   Numerical results

In this section we provide some numerical results to assess the sensitivity of the solution with respect to the parameter accounting for the surrounding tissue in the 1D model (Section 5.1) and carry out several numerical simulations in real geometries for the coupled problem 3D-FSI/1D highlighting its accuracy with respect to the full 3D-FSI problem (Section 5.2).

In all our numerical experiments, we consider the linear elastic structure law given by (1) and we use P1-P1 stabilized finite elements [4] for the fluid, and P1 elements for both the structure as well as the 1D model. We also consider a first order semi-implicit scheme for advancing in time the fluid equations, a first order implicit scheme for the

structure, and a second order explicit Taylor-Galerkin scheme for the 1D model [14]. By taking a time step equal to Δt for the 3D-FSI problem, we use $\Delta t/1000$ for the 1D model, in order to guarantee the stability of the explicit scheme used for the latter problem. At the outlet of the 1D models we consider absorbing boundary conditions [9]. The 3D-FSI model is solved with a preconditioned monolithic strategy, with an explicit treatment of the fluid convective term and of the fluid geometry non-linearity [5]. For the solution of 3D-FSI/1D coupling, we consider the partitioned procedure described in Algorithm 1. To this aim let $\mathcal{F}_{FS}(\boldsymbol{u}_f, p, \boldsymbol{\eta}_s, \boldsymbol{u}_m) = 0$ be the 3D-FSI problem (2), (3), (1), (4), (5), (17), with suitable boundary conditions on $(\cup_j \Sigma_{f,j}) \bigcup (\cup_j \Sigma_{s,j}) \setminus \Gamma_f$, depending on the test at hand, and let $\mathcal{F}_{1D}(Q, A, P) = 0$ be the 1D model (6), (7), (8), (9), with absorbing boundary conditions at $z = L$. Moreover, we denote with Ω^n the approximation at time t^n of domain Ω. We avoid to indicate the superscript ^{n} for the unknowns to avoid confusion with the subiteration index k.

Algorithm 1.

Given the quantities at previous time steps and a tolerance ε, set $Q^{(0)}(t^{n+1})|_{z=0} = Q(t^n)|_{z=0}$. While

$$\left| Q^{(k-1)}|_{z=0} - Q^{(k-2)}|_{z=0} \right| + \left| U^{(k-1)}|_{z=0} - U^{(k-2)}|_{z=0} \right| \geq \varepsilon, \tag{20}$$

solve at each time step t^{n+1} the following problems:

1. Fluid-structure interaction problem

$$\begin{cases} \mathcal{F}_{FS}(\boldsymbol{u}_f^{(k)}, p^{(k)}, \boldsymbol{\eta}_s^{(k)}, \boldsymbol{u}_m^{(k)}) = 0, \\ \int_\Gamma \boldsymbol{u}_f^{(k)} \cdot \boldsymbol{n} \, d\gamma = Q^{(k-1)}|_{z=0}; \end{cases}$$

2. 1D problem

$$\begin{cases} \mathcal{F}_{1D}(Q^{(k)}, A^{(k)}, P^{(k)}) = 0, \\ P^{(k)}|_{z=0} = \dfrac{1}{|\Gamma_f^n|} \int_{\Gamma_f^n} \boldsymbol{T}_f(\boldsymbol{u}_f^{(k)}, p^{(k)}) \boldsymbol{n} \cdot \boldsymbol{n} \, d\gamma + \dfrac{\rho_f}{2} \left(\left(U^{(k-1)}|_{z=0} \right)^2 - \dfrac{1}{|\Gamma_f^n|} \int_{\Gamma_f^n} |\boldsymbol{u}_f^{(k-1)}|^2 \, d\gamma \right). \square \end{cases} \tag{21}$$

Algorithm 1 is based on the prescription of the flow rate to the 3D-FSI model and of the mean total normal stress to the 1D model. For the latter condition, the terms involving the velocities have been computed at previous subiteration. In this way, we rely to a classical pressure conditions for the 1D model. Condition (21) is consistent with $(15)_2$ so that, if convergence is achieved, Algorithm 1 allows to prescribe the preserving energy conditions (15). No theoretical results are nowadays available regarding the convergence of Algorithm 1. However, the numerical results presented in this work show that it is always achieved. We also notice that in the stopping criterion (20) the first term allows

to check the satisfaction of the flow rate condition $(15)_1$, whereas the second one that of the total normal stresses $(15)_2$. For the prescription of a flow rate condition, in this work we considered the Lagrange multipliers approach introduced in [10].

Finally, in all our numerical tests we consider the following values: $\rho_f = 1.04\,g/cm^3$, $\rho_s = 1.2\,g/cm^3$, $\hat{\nu} = \nu = 0.45$, $\alpha = 9$ and a space discretization parameter for the 1D model $h = 0.1\,cm$. All the numerical results have been obtained using the parallel Finite Element library LIFEV developed at MOX - Politecnico di Milano, INRIA - Paris, CMCS - EPF of Lausanne and Emory University - Atlanta [1].

5.1 Effect of the surrounding tissue in the 1D model

In this section, we compare the solution obtained by neglecting the surrounding tissue (ST) in the 1D model (that is by taking $\hat{E} = E$) with that obtained by including it (that is by taking $\hat{E}$ given by (19)).

For the 3D-FSI problem, we consider a cylindrical domain with radius equal to $0.5\,cm$, length equal to $5\,cm$ and structure thickness $H_s = 0.05\,cm$, and we prescribe the flow rate

$$Q = \begin{cases} sin^2(\pi\,t/T) & t \leq T/2, \\ 0 & t > T/2, \end{cases}$$

with $T = 0.008\,s$, at the inlet, whilst we considered a coupling with a 1D model at the outlet.

We consider two cases: $\alpha_e = 10^6\,dyne/cm^3$ and $\alpha_e = 5 \cdot 10^6\,dyne/cm^3$. We also use $\Delta t = 0.001\,s$, $E = 2 \cdot 10^6\,dyne/cm^2$, and, for the 1D model, $L = 5\,cm$, $\widetilde{A} = 0.78\,cm^2$ and $\widehat{H}_s = 0.05\,cm$, the last two values being chosen in order to guarantee the continuity with those of the 3D-FSI model.

In Figure 5 we show the mean pressure at the section located at $2.5\,cm$ from the inlet, obtained by either including or neglecting ST in the 1D model. In particular, Figure 5, left, shows the case $\alpha_e = 10^6\,dyne/cm^3$, whilst Figure 5, right, the case $\alpha_e = 5 \cdot 10^6\,dyne/cm^3$. In both cases, we observe that there is a difference between the two solutions. In particular, the case obtained by neglecting ST in the 1D model features higher spurious reflections due to the mismatch of elastic properties with the 3D model. On the contrary, the case obtained by using (19) features no or very little reflections, as expected. We also notice that the reflections are higher in the case $\alpha_e = 5 \cdot 10^6\,dyne/cm^3$. This is easily explained by noticing that for this case from (19) we have $\hat{E} = 2.19 \cdot 10^7\,dyne/cm^2$, whilst for the case $\alpha_e = 10^6\,dyne/cm^3$ we have $\hat{E} = 5.99 \cdot 10^6\,dyne/cm^2$, so that the higher α_e, the greater the difference between E and $\hat{E}$, and therefore the greater the discrepancy between 1D and 3D-FSI models.

These results highlight that if the surrounding tissue is modeled in the 3D-FSI problem, the coupled system is physically consistent provided that (19) is satisfied.

5.2 Comparison between complete and simplified real cases

In this section we consider three sets of simulations, related to two real cases obtained by reconstructing the geometries of two human carotids from MRI images, by using the
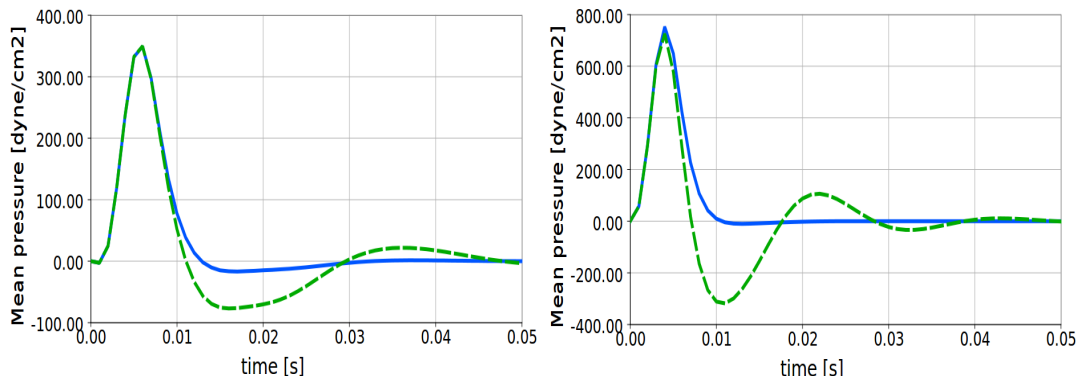
Figure 5: Comparison of the mean pressure at a section far $2.5\,cm$ from the inlet obtained by considering (continuous line) and by neglecting (dash line) the surrounding tissue in the 1D model. $\alpha_e = 10^6\,dyne/cm^3$ (left) and $\alpha_e = 5 \cdot 10^6\,dyne/cm^3$ (right).

package VMTK (http://www.vmtk.org). For each case, we consider the coupling between the model Θ (which changes case by case, see below) and two 1D models at the two outlets of Θ, in particular model *Ext* at the interface with the external carotid and model *Int* at the interface with the internal carotid (see Figure 6, up). Models *Ext* and *Int* have length $L^{Ext} = L^{Int} = 5\,cm$. As for model Θ, we consider three different situations: i) the full 3D-FSI model Ω_F, called in what follows *full model* (FM) (see Figure 6, up, left); ii)-iii) the coupling between the simplified 3D-FSI model Ω_S obtained by cutting a part of the external carotid, and the 1D model *Cut*, representing a reduced model of the cut branch (see Figure 6, up, right). Cases ii) and iii) differ for the choice of the 1D model *Cut*. In particular, in case ii) we consider a constant in space area and thickness, along models *Cut* and *Ext* (simplified model, SM); in case iii) we consider the same values of case i) for model *Ext*, whilst a linear variation in space of area and thickness for model *Cut*, in order to connect with continuity the 3D model and model *Ext* (simplified model with tapering, SMT). To summarize, we report in Table 1 the criteria just described, where with H_s we indicate the mean thickness of the structure at the artificial section Γ_s.

We run the simulations of these three scenarios for three different cases, namely a) patient 1, full domain depicted in Figure 6, middle, left, and simplified model depicted in Figure 6, middle, second subfigure from the left; b) patient 1 with simplified model depicted in Figure 6, middle, third subfigure from the left; c) patient 2, full domain depicted in Figure 6, bottom, left, and simplified model depicted in Figure 6, bottom, second subfigure from the left. The length of the cuts are equal to $1\,cm$ for case a), $1.8\,cm$ for case b), and $0.8\,cm$ for case c).

In Table 2 we report the values of parameters used in the numerical simulations. As for the Young modulus and the parameter describing the ST in the 3D-FSI model, we use the values $E = 3.2 \cdot 10^6\,dyne/cm^2$ and $\alpha_e = 1.1 \cdot 10^6\,dyne/cm^3$. In Table 3 we report the values of the equivalent Young modulus used in the 1D models, accordingly to formula (19).

15

	$\widetilde{A}^{Cut}$	$\widetilde{A}^{Ext}$	$\widetilde{A}^{Int}$	$\widehat{H}_s^{Cut}$	$\widehat{H}_s^{Ext}$	$\widehat{H}_s^{Int}$
FM	X	$\|\widetilde{\Gamma}_{f,F}^{Ext}\|$	$\|\widetilde{\Gamma}_f^{Int}\|$	X	$H_{s,F}^{Ext}$	H_s^{Int}
SM	$\|\widetilde{\Gamma}_{f,S}^{Ext}\|$	$\|\widetilde{\Gamma}_{f,S}^{Ext}\|$	$\|\widetilde{\Gamma}_f^{Int}\|$	$H_{s,S}^{Ext}$	$H_{s,S}^{Ext}$	H_s^{Int}
SMT	$\left(\|\widetilde{\Gamma}_{f,F}^{Ext}\| - \|\widetilde{\Gamma}_{f,S}^{Ext}\|\right)z + \|\widetilde{\Gamma}_{f,S}^{Ext}\|$	$\|\widetilde{\Gamma}_{f,F}^{Ext}\|$	$\|\widetilde{\Gamma}_f^{Int}\|$	$\left(H_{s,F}^{Ext} - H_{s,S}^{Ext}\right)z + H_{s,S}^{Ext}$	$H_{s,F}^{Ext}$	H_s^{Int}

Table 1: Criteria for the choice of the area and the thickness in the 1D models for the three different cases considered. X means that there is no any quantity for the model at hand. The coordinate z refers to model *Cut* with length equal to 1.

	$\|\widetilde{\Gamma}_{f,F}^{Ext}\|$	$\|\widetilde{\Gamma}_{f,S}^{Ext}\|$	$\|\widetilde{\Gamma}_f^{Int}\|$	$H_{s,F}^{Ext}$	$H_{s,S}^{Ext}$	H_s^{Int}
case a)	0.054	0.074	0.082	0.024	0.035	0.040
case b)	0.054	0.083	0.082	0.024	0.035	0.040
case c)	0.092	0.120	0.127	0.020	0.025	0.053

Table 2: Geometrical data used in the numerical simulations. The values of the area are in cm^2, those of thickness in cm.

At the inlet of the 3D-FSI models, we prescribed the physiological flow rate depicted in Figure 7. We imposed homogeneous Dirichlet boundary conditions at the inlet for structure and for harmonic extension problems. At the outlets, for the latter two subproblems we considered homogeneous Neumann conditions. Finally, we set $\Delta t = 0.002\,s$.

In Figures 8 and 9 we show the fluid pressure at the FS interface at two instants, namely $t = 0.06\,s$ (left) and $t = 0.12\,s$ (right), the latter being the systole, obtained for case a) and c), respectively. From these results, we observe that in both cases the 3D pressure fields obtained with SM is quite different with respect to that obtained with FM, here considered as our gold standard. On the contrary, the pressure obtained with SMT is in better agreement with that obtained with FM.

In Figure 10, we show the mean pressure (on the left) and the flow rate (on the right) computed at section Σ_c (depicted in Figure 6, middle and bottom, right), for all the considered cases. These results confirm that the solution obtained with SMT is clearly more accurate than that obtained with SM. This is also confirmed by the maximum mean pressure errors reported in Table 4, which show that for case a) and c) the error of SMT is about three times smaller than that obtained with SM. Figure 10 and Table 4 show also the numerical results obtained for case b). In this case, we can conclude that the
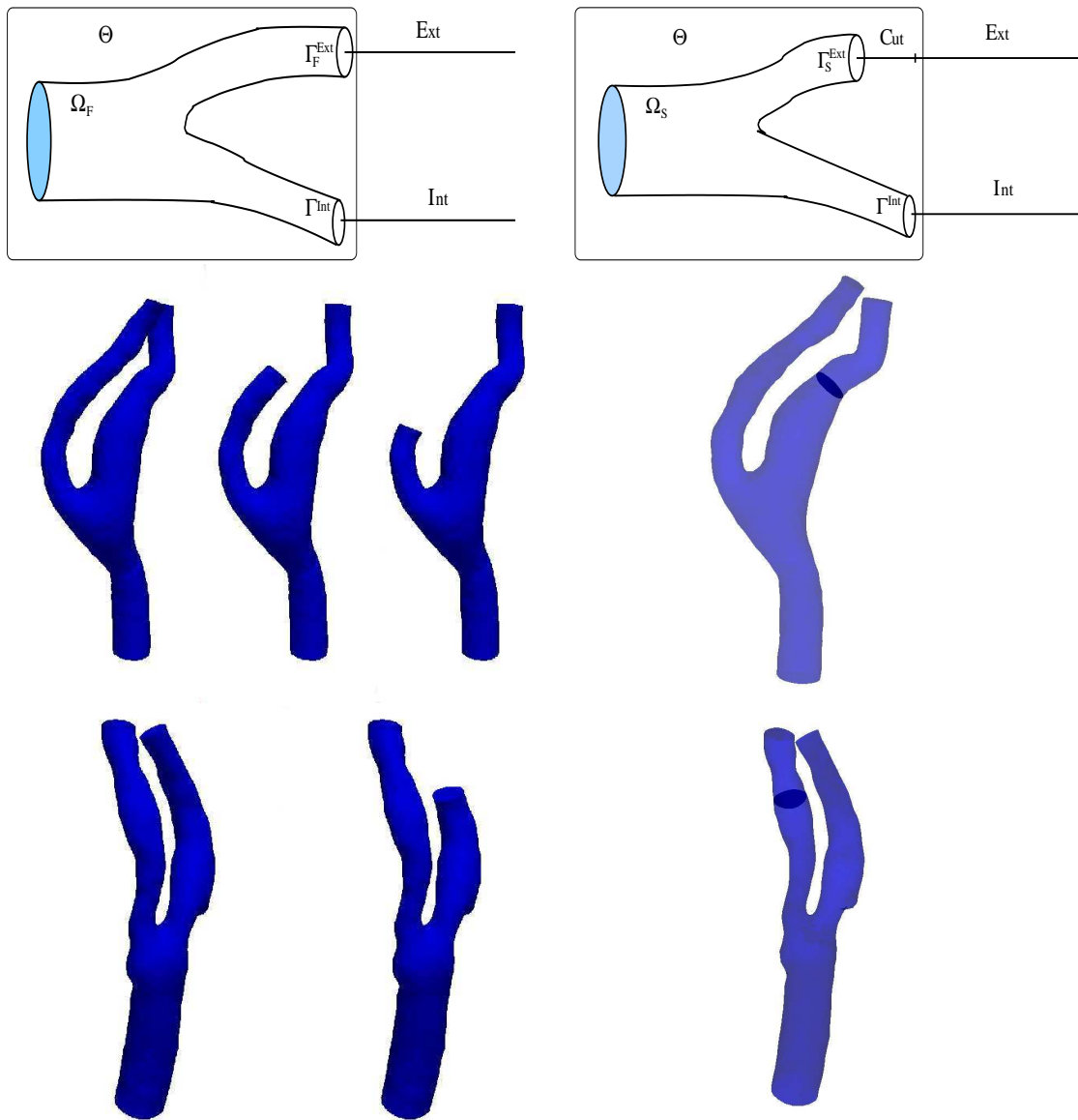
16

Figure 6: Top: schematic representation of the computational domains. On the left the complete model, on the right the reduced one. Middle: geometries for patient 1 (cases a) and b)). Bottom: geometries for patient 2 (case c)). For the last two rows, we report the computational domains, on the left, and the section where the average quantities are computed, on the right.

error featured by SMT seems to be quite independent of the length of the cut, whilst that obtained with SM increases for larger cuts.

		$\widehat{E}^{Cut}$	$\widehat{E}^{Ext}$	$\widehat{E}^{Int}$
	FM	X	3.82	3.80
case a)	SM	3.78	3.78	3.80
	SMT	$0.04\,z + 3.78$	3.82	3.80
	FM	X	3.82	3.80
case b)	SM	3.85	3.85	3.80
	SMT	$-0.03\,z + 3.85$	3.82	3.80
	FM	X	4.47	3.86
case c)	SM	4.53	4.53	3.86
	SMT	$-0.06\,z + 4.53$	4.47	3.80

Table 3: Values ($\times 10^6\,dyne/cm^2$) of the equivalent Young modulus used in the 1D model in the numerical simulations.
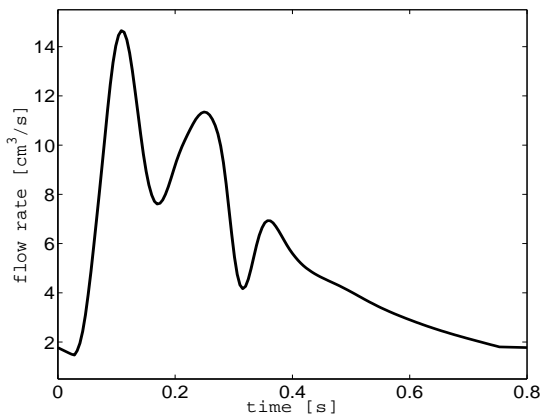
Figure 7: Flow rate prescribed at the inlet of the 3D-FSI model.

6   Conclusions

In this work we dealt with the problem of the physical consistency of the 1D model with respect to the 3D-FSI one, in view of studying the reliability of the coupling between these two models as an effective solution to describe large portions of the vascular tree.

Firstly, we found from our theoretical results that a key ingredient in building consistent coupled models is the satisfaction of an energy preserving principle which has to be satisfied by the interface conditions. For some choices of such conditions we discussed whenever they satisfy this principle. In particular, we found that conditions involving the total pressure are unconditionally energy preserving.

Secondly, we proposed an effective way to introduce the effect of the surrounding tissue in the 1D model, which is mandatory when coupling the 1D with a 3D-FSI model
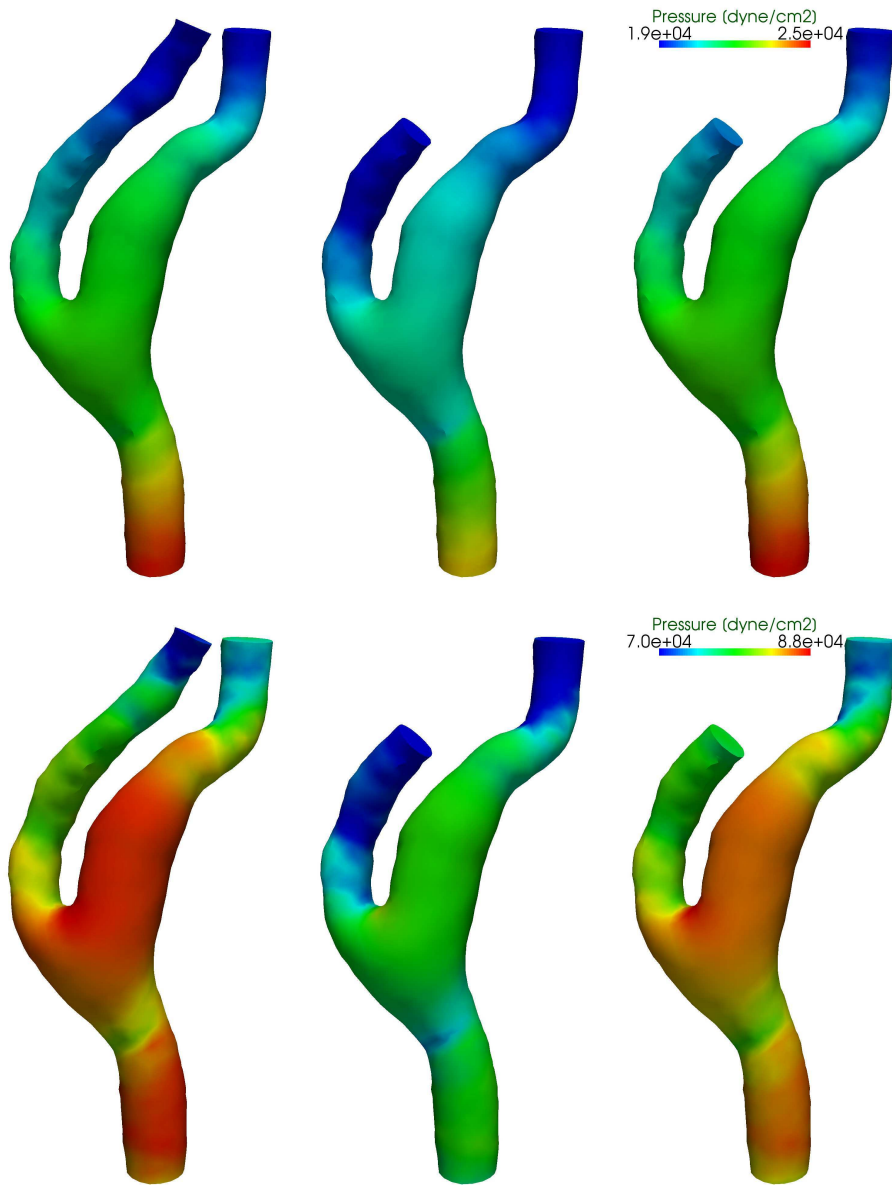
18

Figure 8: Case a). Pressure field at the FS interface at time $t = 0.06\,s$ (up) and $t = 0.12\,s$ (bottom). From left to right we report the three cases FM, SM and SMT.

accounting for the presence of the external tissue. To this aim we introduced an equivalent Young modulus for the 1D model. The numerical results obtained accounting for the ST in the 1D model showed a largely reduced presence of unphysical spurious reflections due to the better matching of the two models.

Finally, we presented several numerical results obtained in real geometries of human
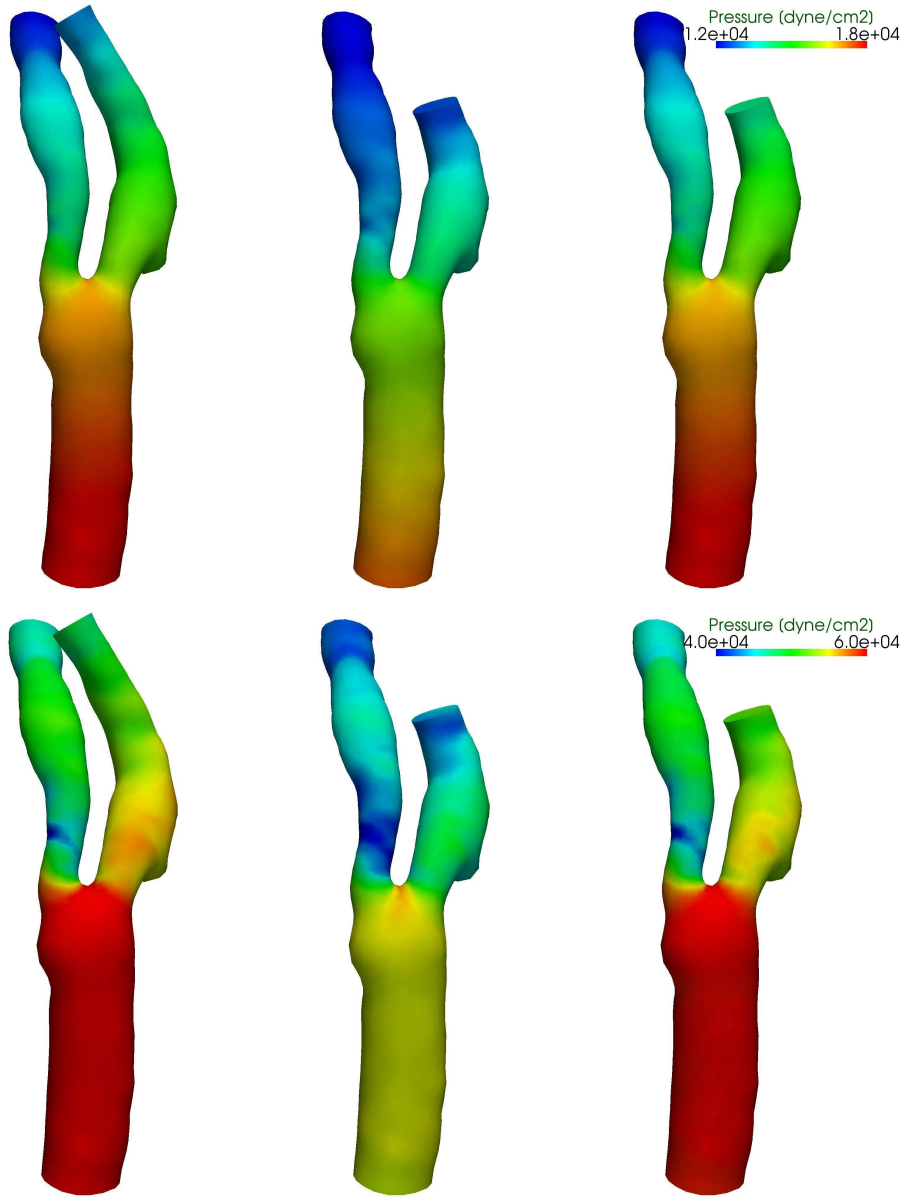
Figure 9: Case c). Pressure field at the FS interfacee at time $t = 0.06\,s$ (up) and $t = 0.12\,s$ (bottom). From left to right we report the three cases FM, SM and SMT.

carotids. These highlighted that by using a tapering in the 1D model in order to take into account the change of vessel diameter, the approximation of the coupled model is enhanced when comparing with the solution obtained with the full model. Moreover, the errors in this case seem to be largely independent of the dimension of the cut.

Our preliminary final conclusions drawn by this work are that the 1D model is an

	SM	SMT
case a)	9.3%	2.3%
case b)	14.0%	2.4%
case c)	10.0%	3.0%

Table 4: Percentage mean pressure maximum errors of simplified models with respect to the full model FM.

effective reduced model of the 3D-FSI provided that total pressure, ST and tapering are considered.
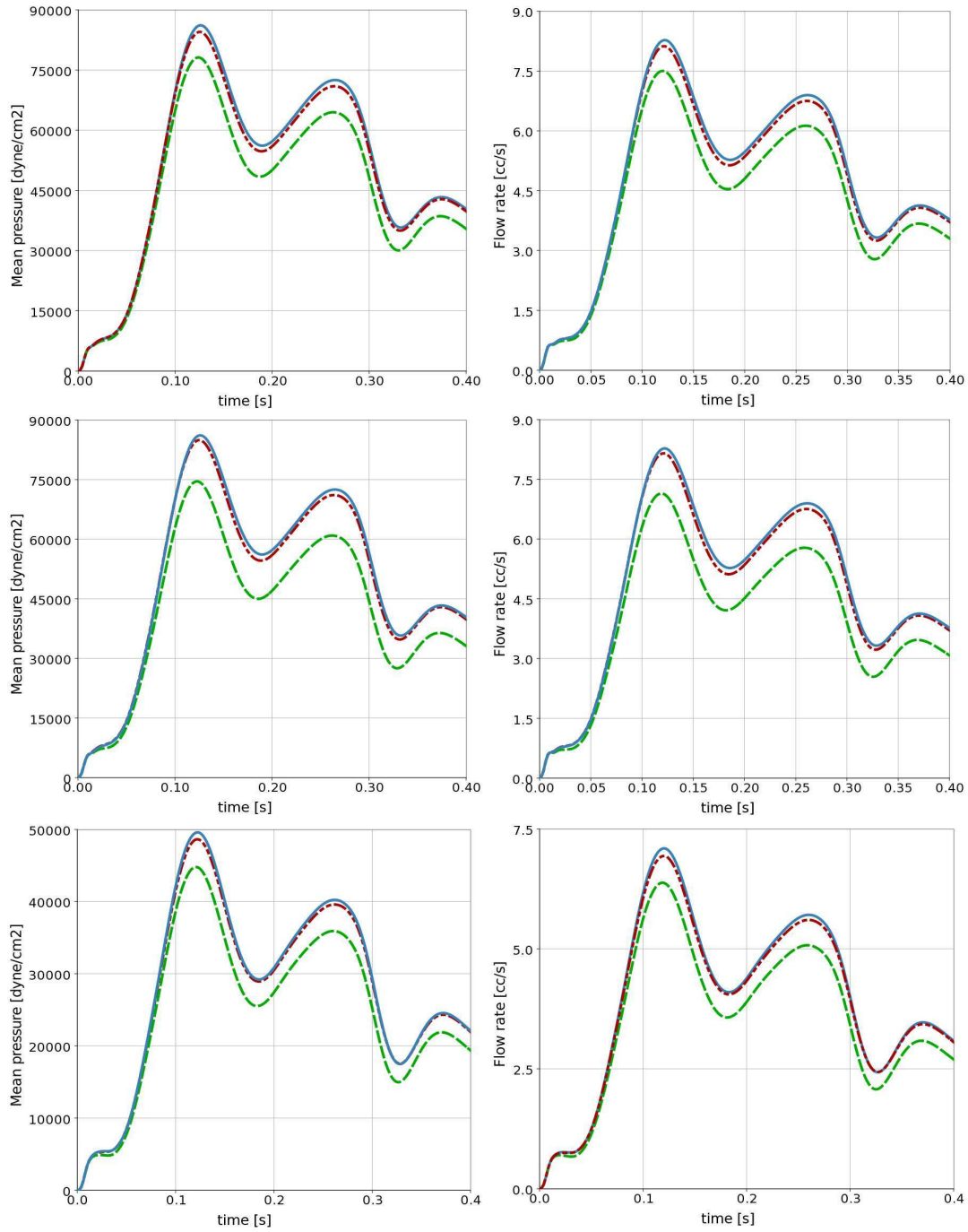
Acknowledgments

Figure 10: Mean pressure (left) and flow rate (right) computed at section Σ_c (see Figure 6, middle and bottom, right). From up to bottom, we show case a), case b) and case c). For each subfigure, we report the solutions obtained with FM (continuous line), SMT (dash-dot line), and SM (dash line).

References

[1] Lifev user manual, `http://lifev.org`, 2010.

[2] P.J. Blanco, R.A. Feijòo, and S.A. Urquiza. A unified variational approach for coupling 3d-1d models and its blood flow applications. *Computer Methods in Applied Mechanics and Engineering*, 196:4391–4410, 2007.

[3] P.J. Blanco, M.R. Pivello, S.A. Urquiza, and R.A. Feijòo. On the potentialities of 3d-1d coupled models in hemodynamics simulations. *J Biomech*, 42:919–930, 2009.

[4] E. Burman and P. Hansbo. Edge stabilization for the generalized Stokes problem: a continuous interior penalty method. *Computer Methods in Applied Mechanics and Engineering*, 195:2393–2410, 2006.

[5] P. Crosetto, S. Deparis, G. Fourestey, and A. Quarteroni. Parallel algorithms for fluid-structure interaction problems in haemodynamics. *SIAM J. Sci. Comput.*, 33:1598–1622, 2011.

[6] P. Crosetto, P. Reymond, S. Deparis, D. Kontaxakisa, N. Stergiopulos, and A. Quarteroni. Fluid-structure interaction simulation of aortic blood flow. *Computers & Fluids*, 43(1):46–57, 2011.

[7] J. Donea. An arbitrary Lagrangian-Eulerian finite element method for transient dynamic fluid-structure interaction. *Computer Methods in Applied Mechanics and Engineering*, 33:689–723, 1982.

[8] L. Euler. Principia pro motu sanguinis per arterias determinando. *Opera posthuma mathematica et physica anno 1844 detecta. Ediderunt P.H. Fuss et N. Fuss Petropoli; Apund Eggers et Socios.*, 1:814–823, 1775.

[9] L. Formaggia, J.-F. Gerbeau, F. Nobile, and A. Quarteroni. On the coupling of 3D an 1D Navier-Stokes equations for flow problems in compliant vessels. *Computer Methods in Applied Mechanics and Engineering*, 191(6-7):561–582, 2001.

[10] L. Formaggia, J.-F. Gerbeau, F. Nobile, and A. Quarteroni. Numerical treatment of defective boundary conditions for the Navier-Stokes equation. *SIAM Journal on Numerical Analysis*, 40(1):376–401, 2002.

[11] L. Formaggia, D. Lamponi, and A. Quarteroni. One-dimensional models for blood flow in arteries. *Journal of Engineering Mathematics*, 47(3-4):251–276, 2003.

[12] L. Formaggia, A. Moura, and F. Nobile. On the stability of the coupling of 3d and 1d fluid-structure interaction models for blood flow simulations. *M2AN Math. Model. Numer. Anal.*, 41(4):743–769, 2007.

[13] L. Formaggia, F. Nobile, A. Quarteroni, and A. Veneziani. Multiscale modelling of the circulatory system: a preliminary analysis. *Comput and Visual in Science*, 2:75–83, 1999.

[14] L. Formaggia, A. Quarteroni, and A. Veneziani (Eds.). *Cardiovascular Mathematics - Modeling and simulation of the circulatory system.* Springer, 2009.

[15] L. Formaggia and A. Veneziani. Reduced and multiscale models for the human cardiovascular system. *Lecture Notes VKI, Lecture Series 2003-07, Brussels,* 2003.

[16] Y. Fung. *Biomechanics: mechanical properties of living tissues.* Springer, 1993.

[17] L. Greenberg, E. Cheever, T. Anor, J.R. Madsen, and G.E. Karniadakis. Modeling blood flow circulation in intracranial arterial networks: a comparative 3d/1d simulation study. *Annals of Biomed Eng,* 39(1):297–309, 20.

[18] G.A. Holzapfel, T.C. Gasser, and R.W. Ogden. A new constitutive framework for arterial wall mechanics and a comparative study of material models. *J Elast,* 61:1–48, 2000.

[19] T. J. R. Hughes, W. K. Liu, and T. K. Zimmermann. Lagrangian-Eulerian finite element formulation for incompressible viscous flows. *Computer Methods in Applied Mechanics and Engineering,* 29(3):329–349, 1981.

[20] Y. Liu, C. Charles, M. Gracia, H. Gregersen, and G. S. Kassab. Surrounding tissues affect the passive mechanics of the vessel wall: theory and experiment. *Am J Physiol Heart Circ Physiol,* 293:H3290–H3300, 2007.

[21] C. Malossi, P.J. Blanco, S. Deparis, and A. Quarteroni. Algorithms for the partitioned solution of weakly coupled fluid models for cardiovascular flows. *Int J Num Meth Biomed Eng,,* In press. DOI:10.1002/cnm.1457, 2011.

[22] F. Migliavacca, R. Balossino, G. Pennati, G. Dubini, T.Y. Hsia, M.R. de Leval, and E.L. Bove. Multiscal modelling in biofluidynamics: application to reconstructive paediatric cardiac surgery. *J Biomech,* 39:1010–1020, 2006.

[23] P. Moireau, N. Xiao, M. Astorino, C. A. Figueroa, D. Chapelle, C. A. Taylor, and J.-F. Gerbeau. External tissue support and fluidstructure simulation in blood flows. *Biomechanics and Modeling in Mechanobiology,* 2011.

[24] F. Nobile, M. Pozzoli, and C. Vergara. Time accurate partitioned algorithms for the solution of fluid-structure interaction problems in haemodynamics. *MOX Report n. 30,* 2011.

[25] A. Quarteroni, M. Tuveri, and A. Veneziani. Computational vascular fluid dynamics: Problems, models and methods. *Computing and Visualisation in Science,* 2:163–197, 2000.

[26] A. Quarteroni and A. Veneziani. Modeling and simulation of blood flow problems. In *Computational Science for the 21st Century,* pages 369–379. J. Periaux et al. eds, J. Wiley and Sons, 1997.

[27] A. Quarteroni and A. Veneziani. Analysis of a geometrical multiscale model based on the coupling of ode and pde for blood flow simulations. *Multiscale Model. Simul.*, 1(2):173–195, 2003.

[28] M. Raghavan and D. Vorp. Towards a biomechanical tool to evaluate rupture potential of abdominal aortic aneurysm: identification of a finite strain constitutive model and evaluation of its applicability. *Journal of Biomechanics*, 33:475–482, 2000.

[29] I. Vignon-Clementel, C.A. Figueroa, K. Jansen, and C. Taylor. Outflow boundary conditions for three-dimensional finite element modeling of blood flow and pressure waves in arteries. *Computer Methods in Applied Mechanics and Engineering*, 195:3776–3996, 2006.